Studies of vibrating atomic force microscope cantilevers in liquid

T. E. Schäffer,[a] J. P. Cleveland, F. Ohnesorge, D. A. Walters, and P. K. Hansma
Department of Physics, University of California, Santa Barbara, California 93106-9530

(Received 19 April 1996; accepted for publication 22 June 1996)

An atomic force microscope (AFM) design providing a focused spot of order 7 μm in diameter was used to analyze the motion of vibrating cantilevers in liquid. Picking an operating frequency for tapping mode AFM operation in liquid is complex because there is typically a large number of sharp peaks in the response spectrum of cantilever slope amplitude versus drive frequency. The response spectrum was found to be a product of the cantilever's broad thermal noise spectrum and an underlying fluid drive spectrum containing the sharp peaks. The geometrical shape of transverse cantilever motion was qualitatively independent of the fluid drive spectrum and could be approximately reproduced by a simple theoretical model. The measurements performed give new insights into the behavior of cantilevers during tapping mode AFM operation in liquid. © *1996 American Institute of Physics.* [S0021-8979(96)01319-9]

INTRODUCTION

Recently, tapping mode in liquids[1–4] was introduced as a new imaging mode for atomic force microscopy (AFM).[5,6] Low lateral forces and a number of other factors make this mode preferable for nondestructive imaging of soft samples such as molecules weakly bound to a surface.[7–11] In tapping mode, a cantilever is vibrated by a piezo actuator and raster scanned over the sample so that the tip is lightly hitting the sample surface. As in related ac modes,[12–15] the oscillation amplitude is monitored and used for feedback.

Submersion in a liquid significantly changes the oscillatory behavior of the cantilevers. For example, resonance frequencies in water are lower than those in air by up to a factor of 5 for the cantilevers used in this work.[16] Quality factors in water are of order 1, compared with 10–100 in air. The reduced resonance frequencies can be explained by the effect of fluid loading that increases the effective mass of the cantilever, while the low quality factors are due to increased hydrodynamic damping.[17,18] However, the presence of the liquid also gives rise to a more complex frequency response than in air when driving the piezo actuator. Many peaks are visible, some quite sharp, that are not cantilever resonances. These peaks have been explained as acoustic vibrations present in the liquid that drive the cantilever.[2] Many of these peaks, not necessarily near cantilever resonances, can be chosen to image the sample in tapping mode, where some work better than others.[2] This leads to the question of how cantilevers move in liquid. The behavior of the fundamental resonance of a cantilever in liquid has been studied[19] and one-dimensional harmonic oscillator theory has been used to model cantilever motion.[20–22] In tapping mode in liquids, however, tapping frequencies are not limited to the cantilever resonances. The cantilever has to be taken as a distributed elastic system with several vibrational modes. Modal shapes in vacuum have been calculated[23,24] and measurements in air are in good agreement with those shapes.[25,26] Recently, a dual optical lever detection system has been introduced that in real-time monitors deformations of the cantilever while scanning.[27]

Here we used a new AFM design, realizing a focused spot size of order 7 μm in diameter. Although this microscope was designed with the goal of using small cantilevers, cantilevers small enough to really test the limits of this microscope are lacking at present. We instead used it to dissect the motion in liquid of a new family of intermediate length cantilevers available to us now.[16]

EXPERIMENTAL METHODS

We used a home-built AFM head (cantilever module and optical beam deflection detection system). It was substituted for a Nanoscope III Multimode head[28] and was used with the Multimode base and scanners, supplemented with analog electronics[29] and a Macintosh-based data acquisition system.[30] It had a focused spot size of 7 μm in diameter, significantly smaller than in commercially available AFMs, in order to measure in detail the motion of small cantilevers. The prototype head had a multicomponent optical system (Fig. 1) similar to those used in interferometric detection systems.[31] A collimated light source, consisting of a 670 nm laser diode coupled to a single-mode optical fiber that terminated with a collimator,[32] produced the incident beam. The incident beam passed through an adjustable aperture that determined the final spot size and was reflected down toward the cantilever by a beamsplitter. Then it passed through a movable lens system and through a polarizing beamsplitter that passed only one polarization direction of the laser light. The other polarization direction was reflected to a beam stop. The light transmitted by the polarizing beamsplitter passed through a $\lambda/4$ wave plate, where it became circularly polarized. The beam reflected by the cantilever passed back through the $\lambda/4$ wave plate; that linearly polarized the reflected beam again, but with a polarization perpendicular to the polarization of the incident beam. This caused the reflected beam from the cantilever to be almost completely reflected by the polarizing beamsplitter onto a segmented photodiode. The polarizing beamsplitter-$\lambda/4$ wave plate assembly is a well-known concept used in interferometry.[31]

[a]Electronic mail: tilman@physics.ucsb.edu

 0021-8979/96/80(7)/3622/6/$10.00

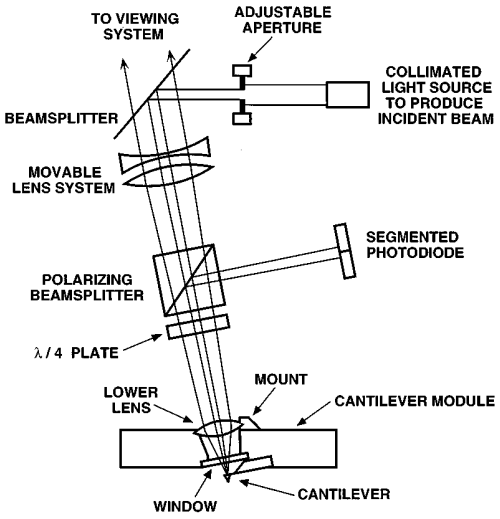

FIG. 1. Optical components of the home-built AFM head. The collimated incident beam from a fiber-coupled laser diode passes through an adjustable aperture that determines the final spot size and is focused onto the cantilever. The reflected beam is separated from the incident beam and is directed toward the segmented photodiode by the polarizing beamsplitter. Mounting the lower lens into the cantilever module is one way to obtain the high numerical apertures that are necessary for small spot sizes. Focusing is simplified by having a viewing system that has infinity-corrected optics and thus is confocal with the incident beam.

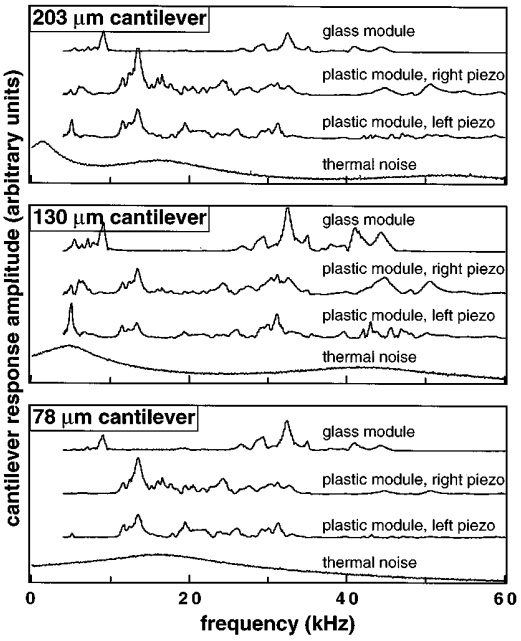

FIG. 2. Cantilever response spectra and log(thermal noise spectra) for various cantilevers and cantilever modules. For different cantilever modules (glass vs plastic), inherently distinct response spectra are obtained. For the same cantilever module (plastic) but different piezo actuators, similar spectra are obtained. Response spectra of different cantilevers in the same module, driven with the same piezo actuator, resemble each other closely. They differ only in the amplitudes of their peaks. Peaks seem to be enhanced where the cantilever's respective noise spectrum has a peak.

Two piezo actuators were built into the head, underneath the feet on which the cantilever module was positioned.

A small spot size requires a large numerical aperture of the focusing optics, which also results in a small depth of focus.[33] If one defines the depth of focus as the range in which the beam spreads by 10% of the spot size, then for a 7 μm spot size the depth of focus is of the order of 50 μm. Due to differences in cantilever substrate thickness and variability in mounting the cantilever, one may have to refocus the incident beam on each cantilever, requiring a high quality viewing system. Since the incident beam is collimated before reaching the movable lens system, infinity-corrected optics are needed for the viewing system to be confocal with the incident beam. In our current implementation a telescope focused at infinity is used, although we have also used a video system. Now, if one adjusts the movable lens system such that the cantilever appears in focus in the viewing system, then, automatically, the incident beam is focused in the plane of the cantilever as well. This is convenient for operating small cantilevers, for which focus is more critical than for large cantilevers. At the same time, the spot from the incident beam can be seen in the viewing system and can be positioned accurately on the cantilever.

As is shown in Fig. 1, the optical axis of the incident beam is tilted from the vertical so that the incident beam is normal to the plane of the cantilever. This has several advantages. For example, the light lost by shadowing from the edge of the chip on which the cantilever is mounted is minimized. This is especially important for the high numerical aperture systems that are necessary for small spot sizes, because a cone of light with a large opening angle must reach the cantilever. Also, the plane of the cantilever is in the plane of focus, thus, one can focus on the cantilever and then move the spot on the cantilever without having to refocus. To avoid complex lens systems or an accumulation of lenses in close proximity to the cantilever, incident and reflected light are overlapped and taken through the same lower lens, after which they are separated by the polarizing beamsplitter.

For our first measurements described in this article, a cantilever chip was mounted in a plastic cantilever module and submerged in purified water. This chip had five rectangular cantilevers of various lengths next to each other.[16] Their dimensions were 78–203 μm in length, 20 μm in width, and 0.44 μm in thickness. The spot was moved towards the tip of a cantilever and the reflected beam was centered on the segmented photodiode such that the difference signal was zero. Cantilever response spectra were taken by applying a sinusoidal voltage to one of the piezo actuators and recording the amplitude of the photodiode difference signal while ramping the piezo frequency (''cantilever tune'' in the Nanoscope software), giving a measure of the frequency-dependent cantilever slope amplitude. This was done for each of the piezo actuators, for three of the cantilevers (Fig. 2). Our ac/dc conversion circuit had a low-frequency rolloff at about 10 kHz. Response spectra of the same cantilevers were also recorded in a glass cantilever module with the commercial multimode head.

Thermal noise spectra for each cantilever were acquired by sampling the amplified photodiode difference signal at high speeds (2^{20} data points with a sampling period of 2.4 μs) and Fourier transforming this data (Hanning windows

with 2^{13} points). The resulting thermal noise spectra for the three different length cantilevers are displayed in semilogarithmic presentation (Fig. 2), so that higher modes can be seen more clearly, whereas the driven cantilever response spectra are on a linear scale, as usually displayed (e.g., by Nanoscope software).

To measure the geometrical shapes of the vibrating cantilevers, the laser spot was moved along a cantilever and response spectra were acquired at several positions between the base and the tip of the cantilever. At each position, the reflected beam had to be recentered on the segmented photodiode by zeroing the dc difference signal, in order to compensate for an overall bending of the cantilever due to internal material and/or thermally induced static stresses. The spot could be positioned with roughly 3 μm accuracy. This measurement provides information on the frequency-dependent slope amplitude of the cantilever oscillation at different positions and thus gives a map of the transverse vibrational shapes of the cantilever slope.

EXPERIMENTAL RESULTS

The most characteristic feature of the cantilever response spectra in Fig. 2 is the ''forest of peaks,'' seen with both the glass and plastic cantilever modules. This forest of peaks is well known to anyone applying tapping mode AFM in liquids. For tapping mode operation, one usually selects an operating frequency on or to the side of one of those peaks in the ''cantilever tune.'' For the same cantilever mounted in different cantilever modules, distinct cantilever response spectra are obtained, as can be seen by comparing the glass to the plastic module. The peaks are at totally different locations. However, for a cantilever in the same (plastic) cantilever module, driving with piezo actuators at different locations on the module results in more similar response spectra. Some peaks, although of different relative heights, occur at the same frequencies while others occur in the same frequency ranges. Similar response spectra were also obtained with different fluid levels. This suggests that geometry and material of the cantilever module contribute to the basic structure of the cantilever response spectrum in the observed frequency range.

The thermal noise spectra are also shown in Fig. 2. The 203 μm cantilever used in these measurements in water has a fundamental frequency, f_0, at about 2 kHz, and the second and third normal modes at 18 and 53 kHz. In air, $f_0 = 1.02/(2\pi)\ \sqrt{E/\rho}\ b/L^2$, where b is the thickness, L is the length, E is the Young's modulus, and ρ is the density.[23] Therefore, shorter cantilevers with the same thickness have higher resonant frequencies. To a first approximation, each mode can be described as an independent simple harmonic oscillator[16,34] with its own effective spring constant, k_n, and its own quality factor, Q_n. By the equipartition theorem, the mean energy $\langle E_n \rangle = k_B T$ couples to a harmonic oscillator in thermal equilibrium. Thus, there are peaks in the thermal noise spectrum at the cantilever's normal mode frequencies, where k_n and Q_n determine the shape of the peaks (in the above approximation). The damping, which reduces the quality factor Q_n to the order of unity and flattens the thermal noise peaks, arises mostly from fluid damping.

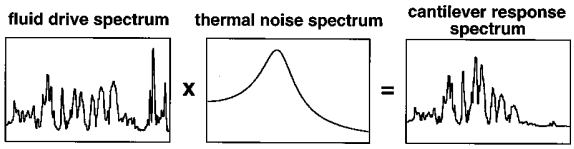

FIG. 3. Schematic illustration of the hypothesis that the cantilever response spectrum is a product of the fluid drive spectrum and the cantilever's thermal noise spectrum. The fluid drive spectrum is a measure of the motion of the fluid close to the cantilever and depends only on the cantilever module, the piezo actuator and the fluid. The thermal noise spectrum depends only on the individual properties of the cantilever in the fluid.

By observing the response spectra of different cantilevers on the chip in the same environment (same module and piezo), one sees strong similarities: the peaks are all at the same frequencies and vary only in relative heights (Fig. 2). Furthermore, peaks for a particular cantilever seem to be enhanced where the cantilever's thermal noise spectrum has a peak. These observations led us to the hypothesis that the cantilever response spectrum is the product of a fluid drive spectrum, which depends only on the cantilever module and fluid, and the thermal noise spectrum, which depends only on the cantilever and fluid (Fig. 3).

In Fig. 4, we further investigate this hypothesis. The response spectra of the 203, 130, and 78 μm cantilevers in the plastic module, driven with the right piezo, are pointwise divided by their respective thermal noise spectra. The resulting spectra, which we call ''fluid drive spectra,'' are scaled by multiplying each by a constant scaling factor. The scaling factor was chosen such that the integral over the square of each spectrum as a function of frequency is identical, thus approximately matching the peak amplitudes. The resulting three spectra resemble each other extremely well. The differences in relative amplitudes in the response spectra disappeared after this division by the respective thermal spectra. Similar observations were made for the other arrangements of Fig. 2 (data not shown). This is strong support for our hypothesis.

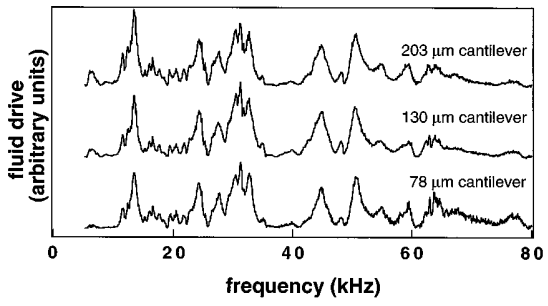

FIG. 4. Fluid drive spectra for adjacent cantilevers. These curves arise from pointwise divisions of the cantilever response spectra by the respective thermal noise spectra (Fig. 2). Their similarity supports the hypothesis from Fig. 3. Each cantilever couples to the same fluid drive in a way approximately described by its thermal noise spectrum (up to a scaling factor).

Further, there is evidence that the cantilevers are driven by an underlying acoustic motion of the fluid rather than by the vibration of the chip since the number of sharp peaks is largely reduced after removing the fluid and since the piezo actuator could be placed almost anywhere in the vicinity of the cantilever without losing the peaks. The fluid drive couples to each cantilever in approximately the same way. We note that we do not know the spatial character of the fluid motion in detail and how this affects the motion of the cantilevers. We also note that an *a priori* more realistic hypothesis would include a different scaling factor for each mode in the thermal noise spectrum. This would correct for differences in the thermal driving force on different cantilever modes and provide an even better approximation to the transfer function of the cantilever.

To further investigate the question of how a cantilever moves in response to the fluid drive, cantilever response spectra $A(f,x)$ were acquired at several positions x between the base $(x=0)$ and the tip $(x=L)$ of the cantilever, meaning that the transverse geometrical shapes of the vibrating cantilever were recorded as a function of drive frequency. For example, cantilever response spectra measured at the end of the cantilever, $x \approx L$, were presented in Fig. 2. $A(f,x)$ is proportional to the slope amplitude of the cantilever at position x during its oscillatory motion at frequency f. The actual geometrical shape could be constructed by piecewise integration. We decided, however, to work with the raw data, $A(f,x)$, i.e., the ''shape'' of the cantilever slope, since it contains all the information needed for our discussion.

In Fig. 5, we plot the normalized slope amplitude $A(f,x)/A(f,L)$, a map of the shape of the cantilever slope dependent on position and frequency. This is possible even at frequencies where both $A(f,x)$ and $A(f,L)$ are small, since enough amplitude is still detected to obtain a measure of the ratio. There are no peaks as in the cantilever response spectra of Fig. 2, and the normalized slope varies smoothly with frequency. Thus, within our experimental accuracy, this normalization effectively divides out the fluid drive spectrum that accounts for different cantilever excitations at different frequencies and shows that the shape of the moving cantilever does not depend on the fluid drive spectrum, even though the amplitude of motion does.

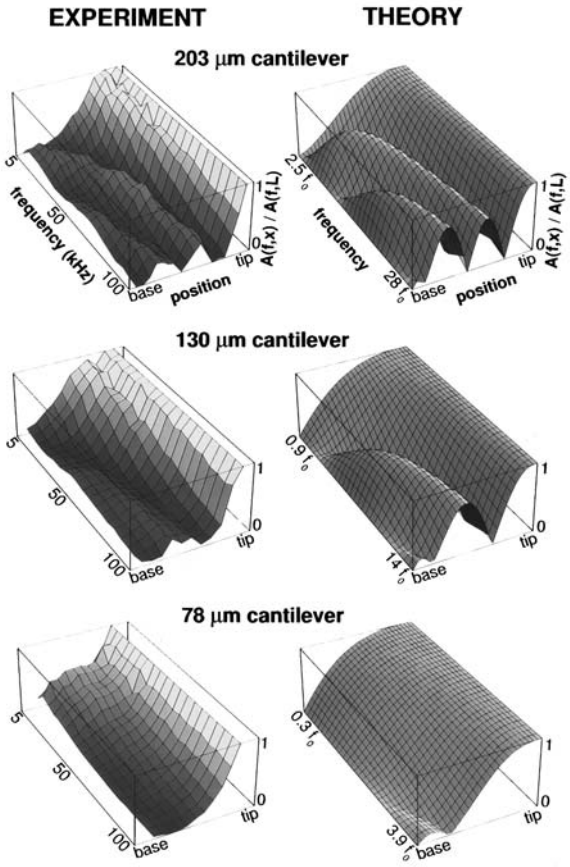

FIG. 5. Experimental and theoretical shapes of cantilever motion, plotted as normalized slope amplitude vs frequency and position. The smoothness of the frequency dependence of the normalized experimental shapes is striking, showing that the shape of the cantilever motion is independent of the fluid drive spectrum at the frequencies investigated. The fluid drive peaks of Fig. 4 do not change the shape of cantilever motion, only its amplitude. Theoretically calculated shapes resemble the measured ones in their basic features: nodal lines develop at the base of the cantilever and move toward the tip for increasing frequencies. At the tip, the slope is always the highest. These similarities show that driven cantilever motion in liquid can be understood qualitatively with our simple model.

DISCUSSION

We constructed a simple theoretical model of a uniform cantilever beam driven by fluid motion. Since the wavelengths of acoustic fluid motion in bulk liquid (15 mm at 100 kHz) are much larger than the cantilevers, we assumed for the model that the spatial variation of this motion on the length scale of the cantilevers is small. Thus the acoustic fluid motion induced by the piezo actuator is approximated as a uniform harmonic drive to the cantilevers (in phase at all points). This drive adds an inhomogeneity to the homogeneous beam equation (Appendix). The solution to this equation yields the slope amplitude $A(f,x)$ of the cantilever. As before, we plot $A(f,x)/A(f,L)$, the normalized slope amplitude of the cantilever motion. These results from the theory are also shown in Fig. 5. Since $A(f,x)$ contains unknown coefficients related to complex fluid loading and coupling effects of the cantilever, it is difficult to work with absolute values of the frequency f in the theoretical plots. Thus, the frequency axis is scaled in multiples of f_0, the fundamental resonance frequency of the cantilever. The low frequency end was matched to the experimental data by setting it to the same multiple of the fundamental frequency as the initial value in the experimental plot. For example, the 203 μm cantilever has a fundamental frequency $f_0=2$ kHz. Since the experimental plot starts at 5 kHz, at 2.5 times the fundamental frequency, the theoretical plot starts at 2.5 f_0. The high frequency end was chosen so that the resulting plot most closely resembles the experimental data plot. We note that the closest resemblance comes for a lower frequency in the theory compared with the experiment, which we believe is due to fluid loading.

There are many similarities between the experimental and the theoretical plots. For low frequencies, up to the fundamental, the normalized slope amplitude increases monotonically from the base to the tip. For increasing frequencies,

nodal lines develop at the base and move toward the tip. At all frequencies, the slope amplitude at the tip is the highest (this is true for the slope amplitude, the derivative of the actual geometrical shape; the actual geometrical shape itself can have a node at the tip).

The profile of each nodal line is distorted in the experimental plot by the shedding of fluid loading mass at higher frequencies.[35] This pushes any feature in the experimental plot to a higher multiple of f_0 than in the theoretical plot (which neglects fluid loading). For example, three nodes of the 203 μm cantilever were observed at 100 kHz=50 f_0, but matched in shape the theoretical curve at 28 f_0.

A subtle discrepancy that was observed for all cantilevers, is that the peak values of the normalized slope amplitude between the base and the tip are 70% of the normalized slope amplitude at the tip for the theoretical model, but less than 50% for the experimental data. We cannot explain this, but systematic discrepancies are expected given the simple nature of the theoretical model. For instance, the presence of a pyramidal tip at the end of the cantilever and the shading of fluid motion by the chip were neglected.

For comparison, we also calculated the shape of the cantilever beam when driving with a localized force at the tip. This variation, however, inherently changed the behavior of the nodal lines: Instead of developing at the base and moving toward the tip for increasing frequencies, they developed at the tip and moved towards the base. This shows that the forces driving the cantilever are not localized at the tip.

CONCLUSION

We built an AFM head with optical beam deflection detection and a focused spot size of 7 μm that is capable of detecting and dissecting the motion of small cantilevers. The spot was focused on the cantilever with a viewing system that was confocal with the optical beam deflection system: when the cantilever is in focus in the viewing system, the spot is in focus on the cantilever. Response spectra for different size cantilevers with different cantilever modules and piezo actuators at different positions revealed that the cantilever response spectrum is approximately a product of the cantilever's thermal noise spectrum and the fluid drive spectrum. Moreover, the geometrical shapes of the vibrating cantilever were found to be independent of the fluid drive, and thus only dependent on cantilever properties in the fluid. These shapes were compared to a simple theoretical model.

ACKNOWLEDGMENTS

This work was supported by a grant from the Materials Research Division of the National Science Foundation (current grant No. NSF DMR 9622169) and a Feodor Lynen Fellowship by the Humboldt Foundation (FO). We thank Digital Instruments for AFM support.

APPENDIX

Free, undamped, transverse vibrations of a uniform rectangular beam can be described by the homogeneous partial differential equation

$$\rho b w \frac{\partial^2 z}{\partial t^2} + EI \frac{\partial^4 z}{\partial x^4} = 0, \tag{A1}$$

where b is the thickness, w is the width, I is the moment of inertia, ρ is the density, and E is the Young's modulus of the beam.[23] If we drive the beam with a uniform harmonic pressure $P = P_0 \sin(2\pi f t)$ over its surface, the differential equation becomes inhomogeneous and can be written as

$$\rho b w \frac{\partial^2 z}{\partial t^2} + EI \frac{\partial^4 z}{\partial x^4} = w P_0 \sin(2\pi f t). \tag{A2}$$

Postulating $z(x,t) = u(x)\sin(2\pi f t)$ yields a spatial part,

$$\frac{d^4 u}{dx^4} - \kappa^4 u = \frac{w P_0}{EI}, \quad \text{where} \quad \kappa^4 = \frac{4\pi^2 \rho b w}{EI} f^2. \tag{A3}$$

The general solution to the spatial part is

$$u(x) = \frac{-w P_0}{EI\kappa^4} + C_1 \sin(\kappa x) + C_2 \sinh(\kappa x) + C_3 \cos(\kappa x) + C_4 \cosh(\kappa x). \tag{A4}$$

For a cantilever beam of length L, clamped at $x=0$ and free at $x=L$, the boundary conditions are

$$u(0)=0; \quad \frac{\partial u}{\partial x}(0)=0; \quad \frac{\partial^2 u}{\partial x^2}(L)=0; \quad \frac{\partial^3 u}{\partial x^3}(L)=0. \tag{A5}$$

Applying the boundary conditions (A5) to (A4) leads to a set of four equations for the quantities C_{1-4}. In the homogeneous case, they can only be solved for certain eigenfrequencies κ_n and their associated eigenmodes. Here, with the inhomogeneity, with a given κ, we obtain

$$\begin{aligned} u(x) = {} & \frac{P_0}{8\rho b \pi^2 f^2 [1+\cos(\kappa L)\cosh(\kappa L)]} \\ & \times \{-2[1+\cos(\kappa L)\cosh(\kappa L)] + \cos(\kappa x) + \cosh(\kappa x) \\ & + \cos(\kappa L - \kappa x)\cosh(\kappa L) + \cos(\kappa L)\cosh(\kappa L - \kappa x) \\ & - \sin(\kappa L - \kappa x)\sinh(\kappa L) + \sin(\kappa L)\sinh(\kappa L - \kappa x)\}. \end{aligned} \tag{A6}$$

$u(x)$ is the actual shape of the cantilever, dependent on frequency. Note that there is a resonance when $1+\cos(\kappa L)\cosh(\kappa L)=0$; the same condition in the homogeneous case gives the eigenfrequencies κ_n. Simple differentiation of $u(x)$ finally yields the slope amplitude of the beam, $A(f,x) = u'(x)$.

[1] P. K. Hansma, J. P. Cleveland, M. Radmacher, D. A. Walters, P. E. Hillner, M. Bezanilla, M. Fritz, D. Vie, H. G. Hansma, C. B. Prater, J. Massie, L. Fukunaga, J. Gurley, and V. Elings, Appl. Phys. Lett. **64**, 1738 (1994).

[2] C. A. J. Putman, K. O. van der Werf, B. G. de Grooth, and N. F. van Hulst, Appl. Phys. Lett. **64**, 2454 (1994).

[3] M. A. Lantz, S. J. O'Shea, and M. E. Welland, Appl. Phys. Lett. **65**, 409 (1994).

[4] F. Ohnesorge and G. Binnig (unpublished); F. Ohnesorge, dissertation thesis, 1994.

[5] G. Binnig, C. F. Quate, and C. Gerber, Phys. Rev. Lett. **56**, 930 (1986).

[6] D. Rugar and P. Hansma, Phys. Today **43**, 23 (1990).

[7] C. A. J. Putman, K. O. van der Werf, B. G. de Grooth, N. F. van Hulst, and J. Greve, Biophys. J. **67**, 1749 (1994).

[8] M. Bezanilla, B. Drake, E. Nudler, M. Kashlev, P. K. Hansma, and H. G. Hansma, Biophys. J. **67**, 2454 (1994).
[9] A. Vinckier, F. Hennau, K. Kjoller, and L. Hellemans, Rev. Sci. Instrum. **67**, 387 (1996).
[10] M. Radmacher, M. Fritz, H. G. Hansma, and P. K. Hansma, Science **265**, 1577 (1994).
[11] M. Fritz, M. Radmacher, J. P. Cleveland, M. W. Allersma, R. J. Stewart, R. Gieselmann, P. Janmey, C. F. Schmidt, and P. K. Hansma, Langmuir **11**, 3529 (1995).
[12] M. Dreier, D. Anselmetti, T. Richmond, U. Dammer, and H. J. Güntherodt, J. Appl. Phys. **76**, 5095 (1994).
[13] R. Erlandsson, G. M. McClelland, C. M. Mate, and S. Chiang, J. Vac. Sci. Technol. A **6**, 266 (1988).
[14] Q. Zhong, D. Inniss, K. Kjoller, and V. B. Elings, Surf. Sci. Lett. **290**, L688 (1993).
[15] D. Anselmetti, R. Luthi, E. Meyer, T. Richmond, M. Dreier, J. E. Frommer, and H. J. Güntherodt, Nanotechnology **5**, 87 (1994).
[16] D. A. Walters, J. P. Cleveland, N. H. Thomson, P. K. Hansma, M. A. Wendman, G. Gurley, and V. Elings, Rev. Sci. Instrum. (in press).
[17] H. J. Butt, P. Siedle, K. Seifert, K. Fendler, T. Seeger, E. Bamberg, A. L. Weisenhorn, K. Goldie, and A. Engel, J. Microsc. **169**, 75 (1993).
[18] G. Y. Chen, R. J. Warmack, T. Thundat, D. P. Allison, and A. Huang, Rev. Sci. Instrum. **65**, 2532 (1994).
[19] S. Inaba, K. Akaishi, T. Mori, and K. Hane, J. Appl. Phys. **73**, 2654 (1993).
[20] D. Sarid, J. Chen, and R. K. Workman, Comp. Mater. Sci. **3**, 475 (1995).
[21] G. Y. Chen, R. J. Warmack, A. Huang, and T. Thundat, J. Appl. Phys. **78**, 1465 (1995).
[22] J. P. Spatz, S. Sheiko, M. Moller, R. G. Winkler, P. Reineker, and O. Marti, Nanotechnology **6**, 40 (1995).
[23] D. Sarid, *Scanning Force Microscopy With Applications to Electric, Magnetic, and Atomic Forces* (Oxford University Press, New York, 1991).
[24] H. J. Butt and M. Jaschke, Nanotechnology **6**, 1 (1995).
[25] D. F. L. Jenkins, M. J. Cunningham, W. W. Clegg, and M. M. Bakusk, Meas. Sci. Technol. **6**, 160 (1995).
[26] U. Rabe, K. Janser, and W. Arnold (unpublished);U. Rabe and W. Arnold, Ann. Phys. **3**, 589 (1994).
[27] H. Kawakatsu, H. Bleuler, T. Saito, and K. Hiroshi, Jpn. J. Appl. Phys. **34**, 3400 (1995).
[28] Digital Instruments, Santa Barbara, CA.
[29] Model 184 and Model 80, Wavetek, San Diego, CA: Model 113, Princeton Applied Research, Princeton, NJ.
[30] NB-MIO-16x, National Instruments, Austin, TX: MacAdios II, GW Instruments, Somerville, MA.
[31] D. Rugar, H. J. Mamin, R. Erlandsson, J. E. Stern, and B. D. Terris, Rev. Sci. Instrum. **59**, 2337 (1988).
[32] Oz Optics, Carp, Ontario, Canada.
[33] M. Born and E. Wolf, *Principles of Optics* (Pergamon, Oxford, 1980).
[34] S. Timoshenko, D. H. Young, and W. Weaver, *Vibration Problems in Engineering* (Wiley, New York, 1974).
[35] L. D. Landau and E. M. Lifshitz, *Fluid Mechanics* (Pergamon, Oxford, England, 1987).